Chemical Physics Impact 2 (2021) 100012

Contents lists available at ScienceDirect

Chemical Physics Impact

journal homepage: www.elsevier.com/locate/chphi

Analysis of the Jahn-Teller effect in coronene and corannulene ions and its effect in EPR spectroscopy

Francesco Tampieri[a,1], Antonio Barbon[a,*], Matteo Tommasini[b,*]

[a] Dipartimento di Scienze Chimiche, Università degli Studi di Padova, Via Marzolo 1, 35131 Padova, Italy
[b] Dipartimento di Chimica, Materiali e Ingegneria Chimica, Politecnico di Milano, Piazza Leonardo da Vinci 32, 20133 Milano, Italy

ARTICLE INFO

Keywords:
Coronene
Corannulene
Electron paramagnetic resonance
Density functional theory
Jahn-Teller
g-tensor

ABSTRACT

Coronene and corannulene are popular structures that have provided the basis for the investigation of extended carbon-based structures, like graphene, fullerene and their derivatives. Here we address the Jahn-Teller (JT) effects in electron paramagnetic resonance (EPR) spectroscopy of such molecules in ionic form. By density functional theory (DFT) and a Monte Carlo based sampling of the potential energy surface, we obtain three and five symmetry-related JT equivalent conformers in coronene and in corannulene ions, respectively. The structure and the interconversion between the JT distorted forms are discussed for their implication in EPR spectroscopy. The calculation of the *g*-tensor by DFT methods has also been benchmarked to serve as methodological approach for the investigation of more extended graphene molecules.

Introduction

Coronene and corannulene are representative members of the family of polycyclic aromatic hydrocarbons (PAHs) compounds. PAHs have attracted (and still attract) considerable scientific and technological interest for a number of different reasons. They provide an ideal ground for the developments of π-bonding theories [1,2] and the assessment of aromaticity in higher PAHs, such as coronene and corannulene, is still matter of research [3,4]. PAHs bear astrophysical relevance since they are thought to be present in interstellar media as charged species [5–10]. The occurrence of PAHs as combustion products and their toxicity raise health and environmental concerns [11].

Due to extended π-conjugation, the optical and electronic properties of PAHs are appealing for materials science [12]. For instance, corannulene behaves as a good electron acceptor, even in solid-state films [13]. Furthermore, the inherent propensity of PAHs to π-stacking (including the case of non-planar corannulene, see for instance the work of Yamada et al. [14]), may drive the self-assembly of structures characterized by useful transport properties for molecular electronics [15–17] and photonics [18].

Another important aspect of PAHs is that they constitute molecular models of graphene, a material with unique properties [19] that has been investigated through several techniques, including electron paramagnetic resonance (EPR) [20]. An effort is put today on the study of real graphene-like systems, with characteristics that lead them far from the ideality of the graphene lattice, such as limited dimensions (*i.e.,* π-conjugation confinement), presence of defects or functional groups, or bending of the planar structure [21,22]. The joint effect of these peculiarities may impart to these systems different properties that can be used to tune the materials toward specific applications. Several theoretical methods have been considered to include these effects (see the work of Kheirabadi and Shafiekhani [23] and references therein). The joint use of density functional theory (DFT) methods and molecular dynamics has shown to be particularly useful for modeling the properties of these systems [24–26]. Furthermore, thanks to advances in computational chemistry software and computers, informative calculations can be carried out on a relatively wide range of molecular sizes, thus making the molecular approach appealing to graphene (*i.e.*, the bottom-up approach) [27].

In the study of molecular graphene, a relatively small number of papers have been published which include EPR investigation of these materials [20,28], as compared to other experimentally available techniques. EPR spectroscopy allows studying paramagnetic centers, also in the presence of ferromagnetic (or antiferromagnetic) exchange interactions. The high selectivity of EPR enables determining the presence of different types of contributions in the spectra of graphene-like samples [20,28–31]. In different kinds of graphite-like materials the typically accessible experimental EPR parameter (*g*-tensor) show a variability of values that has not been yet associated to descriptors of the material

* Corresponding authors.
E-mail addresses: antonio.barbon@unipd.it (A. Barbon), matteo.tommasini@polimi.it (M. Tommasini).
[1] Present address: Biomaterials, Biomechanics and Tissue Engineering Group, Department of Materials Science and Engineering, Technical University of Catalonia (UPC), c. Eduard Maristany 16, 08019 Barcelona, Spain.

https://doi.org/10.1016/j.chphi.2021.100012
Received 14 December 2020; Received in revised form 11 February 2021; Accepted 15 February 2021

structure, such as the presence of edge states, defects, or bending of the graphene flakes [29,32,33]. We believe that this gap is one of the possible reasons that prevented a wider use of EPR in the characterization of graphene-like systems.

In this work, we begin filling this gap, by starting a study of the effects on EPR spectra of what we could define as *perturbations* to the ideal structure of graphene. Unfortunately, the variety of perturbations can be rather wide (*e.g.*, different edge topology, influence of heteroatoms, strain of the honeycomb structure/topological defects, *etc*. [34–36]). For this reason, we decided to focus on the calculation of the *g*-tensor of simple molecules with extended π-conjugation, subject to Jahn-Teller (JT) distortion, considering the effects of curvature, which are caused by a local disruption of the honeycomb motif (*i.e.*, the topological defect caused by the substitution of a hexagonal ring with a pentagonal ring). Due to the availability of experimental and theoretical data to compare with, the chosen molecules are coronene (planar) and corannulene (bent).

Coronene is representative of an H-terminated nano-graphene with lateral dimension of approximately 1 nm. This highly symmetric molecule (D_{6h} point group) possesses degenerate HOMO and LUMO levels, thus undergoing JT distortion upon removal or addition of an odd number of electrons. This issue has been assessed in the 60′s for a series of highly symmetric aromatic ions, like benzene and simple polyaromatics, including coronene. Results from Hückel calculation and EPR measurements of hyperfine interactions and linewidths convey to state that such a distortion is present in the highly symmetric molecules, and that polar solvents play a role on this [37]. Forty years later more accurate DFT calculations by Kato et al. showed that the inclusion of JT distortion affords excellent agreement with experiment in the vibrational frequencies of coronene [38]. However, even if particularly careful and accurate, this study still shows the presence of a slight instability in the potential energy surface with associated imaginary wavenumber modes. The authors, in another work, calculated the vibrational spectrum for corannulene, showing also in that case a removing of the degeneracy of the orbital by a distortion of the molecule [39]. JT effects, in a work by Galué et al., has been shown to be more important for corannulene with respect to coronene [40].

Experimental evidence for the anions was given by the X-ray diffraction analysis conducted by Filatov et al. [41]. A further study by Andjelković et al. calculated vibrational frequencies and determined a very low energy barrier between the symmetry-related JT distorted forms [26].

At first, our present investigation aims at providing geometries with fully stable energy minima of the JT distorted structures of corannulene and coronene ions and to obtain vibrational frequencies to be compared to previously determined experimental geometries and experimental and calculated vibrational frequencies [38]. This will serve for further investigation on the magnetic properties of the molecule, in particular we will consider the calculation of the *g*-tensor, related to experimental observables, and discuss the effect of the JT distortion of both molecules in the anionic and in the cationic forms. The DFT results are critically discussed and compared to available experimental data.

Methods

The neutral ground states of highly symmetric coronene (D_{6h}) and corannulene (C_{5v}) have doubly degenerate HOMOs and LUMOs. Hence, the addition (removal) of one electron to form an ion causes the partial filling of the doubly degenerate LUMOs (HOMOs), which is the classical situation leading to JT distortion. This means that the molecule is prone to change its structure (relax) and reduce its point group symmetry. With this picture in mind, we set a Monte Carlo inspired exploration of the JT structures of the anions and cations of coronene and corannulene in the following way. We began with the reference optimized structures of the neutral ground state (X_0), and we added a small random perturbation (δ_X) whose immediate effect is to slightly lift the degeneracy of the HOMOs and LUMOs, in a way that depends on the particular realization of δ_X. The perturbation added to the position of each atom was defined as a random vector v picked up from a uniform distribution of points on a sphere of radius 0.001 Å. The required random vectors v were evaluated with a convenient approach devised by Marsaglia [42]. The structure $X_0 + \delta_X$ was then taken as the initial structure for tight geometry optimization of the anion/cation species. By repeating the procedure for different random choices of δ_X it is possible to effectively explore the potential energy surface of the JT potential, easily recovering the different equivalent minima. Tight optimization and tight SCF convergence were crucial to get final structures of the expected symmetry [43], with no imaginary vibrational frequencies. For each charged species, about 20 Monte Carlo runs were enough to recover all the expected deformed structures (based on the initial molecular symmetry, see further).

All calculations have been carried out on isolated molecules based on DFT, by considering the widely adopted B3LYP hybrid functional, which is known to provide reliable equilibrium molecular structures (also adopted in the work by Kato et al. [38]). Therefore, we used Gaussian09 with the B3LYP/6–311G(d,p) method. We have then calculated the vibrational frequency for all the optimized structures to assess that they were actual minima (with no negative eigenvalues of the Hessian). These optimized structures were used for the DFT calculations of the *g*-tensors. To this aim, we used the ORCA quantum chemistry code (version 4.2.1) [44] testing several basis sets within the GIAO approach [45] and the RI-JK approximation (def2/JK keyword).

Calculation of the vibrational frequencies

The equilibrium bond length have been obtained by DFT for the neutral coronene in D_{6h} symmetry and have been compared with those computed by Kato et al. [38], and the experimental values [41,46]. The result of this comparison with most accurate data is reported in Table SI1, and it shows a good agreement both considering previous calculations, and experimental values. Therefore, following the procedure described in the Methods section, we have obtained for coronene the three symmetry-related stable equilibrium geometries of both ions (no imaginary frequencies were observed in such JT distorted structures, see Fig. 1). As expected, the three equivalent JT forms of both ions display lower symmetry than the neutral forms (D_{2h} *vs.* D_{6h}) and are related one another by a C_3 rotation around the axis orthogonal to the molecular plane.

The pattern of equilibrium bond length obtained for the JT distorted coronene ions can be justified by considering the spatial distribution of the frontier orbitals (Fig. 2). For instance, the bonds of the anion, which elongate compared to their length in the neutral structure, are all associated to positions where the singularly occupied molecular orbital (SOMO) displays a nodal plane approximately bisecting the bond. In other words, the SOMO introduces antibonding character in these positions, which causes bond elongation passing from the neutral to the anionic form. Conversely, the bonds where the SOMO displays a bonding character are all becoming shorter in the anion compared to the neutral form.

In the case of coronene cation, to rationalize the obtained structure relaxation displayed in Fig. 2, one should consider the orbital from which the electron was formally removed (*i.e.* the HOMOβ). Upon removing of the electron, the orbital becomes a SOMO, and the reduction of density affects the bond lengths: bonds where SOMO is bonding elongates in the cation, because of the removal of the electronic bonding charge. Conversely, the bonds having antibonding contribution from the SOMO become shorter, because of the reduction of this antibonding contribution upon ionization.

Considering the values of the bond lengths changes between the ionic and neutral form, we see from Fig. 2 that the JT distortion affects principally the radial and edge CC bonds of coronene. Due to the placement of the elongating bonds (all aligned along the vertical axis in Fig. 2) in coronene anion the JT distortion causes a net stretching of the molecule along the vertical axis, which leads to the reduction of symmetry from

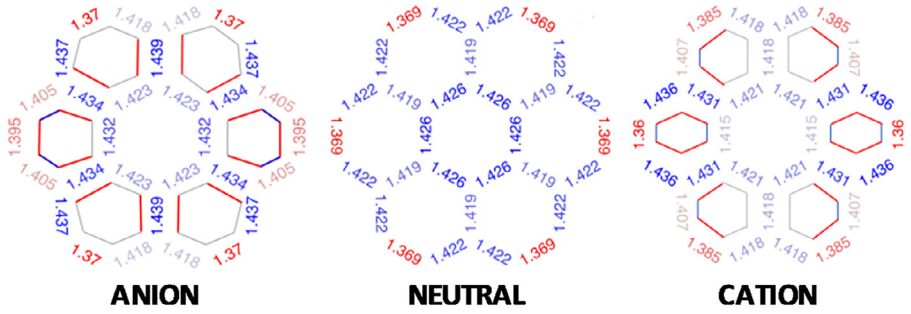

Fig. 1. Bond lengths of one JT distorted equilibrium structure (the other two are symmetry-related obtained by C_3 rotation) of coronene anion (left) and cation (right). The sketched hexagons emphasize the distortion of the rings from the neutral form (blue: shortening, red: lengthening, grey: almost unaffected). The neutral form is shown for reference (centre). (For interpretation of the references to color in this figure legend, the reader is referred to the web version of this article.)

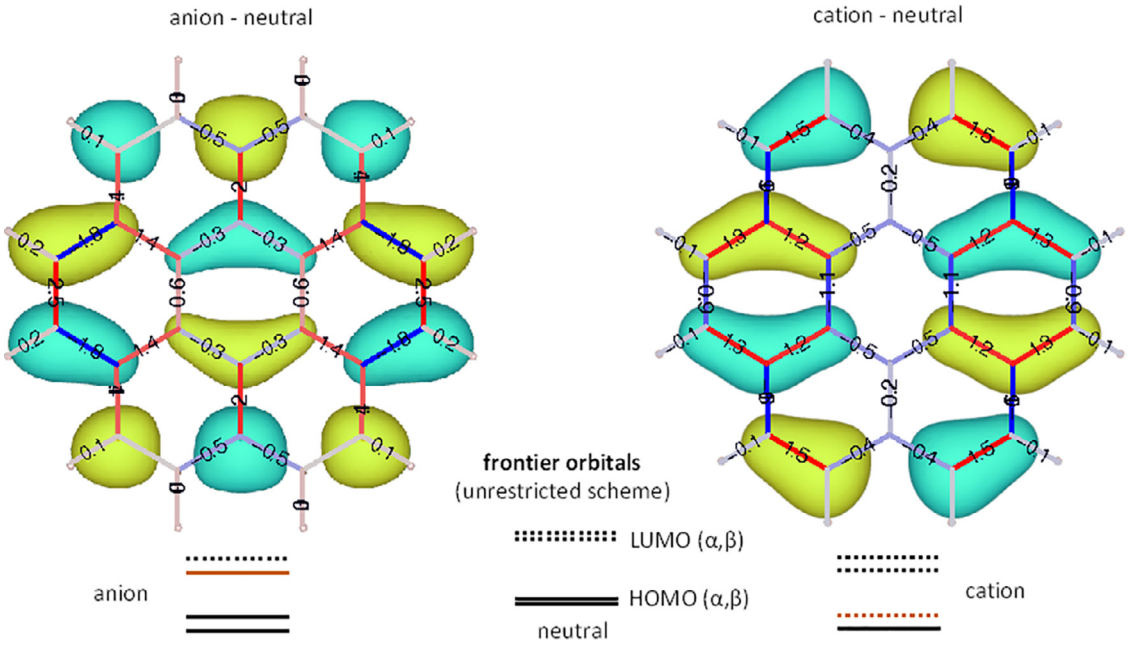

Fig. 2. JT analysis of coronene anion (left) and cation (right): The variation of the bond length with respect to the neutral form (blue bonds correspond to a shortening, and red bonds to an elongation) is shown. Selected frontier spin-orbitals are shown overlapped with each structure to justify the observed structure relaxation patterns (see text and ESI for additional details). The JT distorted structures of the coronene anion and cation both belong to the D_{2h} point group symmetry. The electronic wavefunction of the anion is 2-B_{2g} and that of the cation is 2-A_u. (For interpretation of the references to color in this figure legend, the reader is referred to the web version of this article.)

D_{6h} to D_{2h}. Since there are three equivalent axes along which the stretching of coronene may occur, we count three equivalent JT distorted forms in coronene anion as anticipated earlier.

In the case of coronene cation, compared to the neutral D_{6h} structure, the molecule undergoes a contraction along the vertical axis of Fig. 2, for reasons similar (but opposite) to the case of the anion, and a stretching along the horizontal axis.

We have carried out the same kind of theoretical analysis of the JT distortion also for corannulene, in both anionic and cationic state. Fig. 3 shows the equilibrium structure of one out of the five equivalent JT distorted equilibrium structures of the ionic forms of corannulene (both belonging to C_S point group). These are compared with the equilibrium structure of neutral corannulene (belonging to the C_{5v} point group). The geometry relaxation driven by the JT distortion can be better inspected in Fig. 4, where it is compared with the relevant frontier orbital. This orbital is the one that differs between the charged and the neutral state. Similar to the previous case of coronene, all CC bond changes can be rationalized by the inspection of the nodal pattern of the frontier orbitals of interest. Notably, compared with the equilibrium structure of neutral corannulene, the CC bonds of the anion become shorter where the orbital of the added electron display a bonding character. This is the opposite in the case of the cation: here CC bonds becoming shorter where the orbital of the removed electron has antibonding character (*i.e.* it displays a nodal plane bisecting the bond).

We note that the CC bond variations with respect to the neutral form are slightly higher in corannulene than in coronene (compare Fig. 4 with Fig. 2).

The vibrational structure and IR transitions of the cations of coronene and corannulene have been carefully addressed in the past [26,40,47,48], driven by the interest in PAHs as sources of IR emission bands observed in the astrophysical context [49]. Three mid-IR bands of the coronene cation have been observed in matrix-isolated experiments [50]. The results from previous DFT calculations [47] and those presented in this work correlate very well with such experimental findings, which supports the conclusion that the coronene cation possess just one JT distorted form (Table 1 and Table SI1). The same conclusion was reached by multideterminantal-DFT and intrinsic distortion path methods [26].

Quite remarkably, differently from the coronene cation, the corannulene cation was reported to possess two inequivalent JT distorted forms

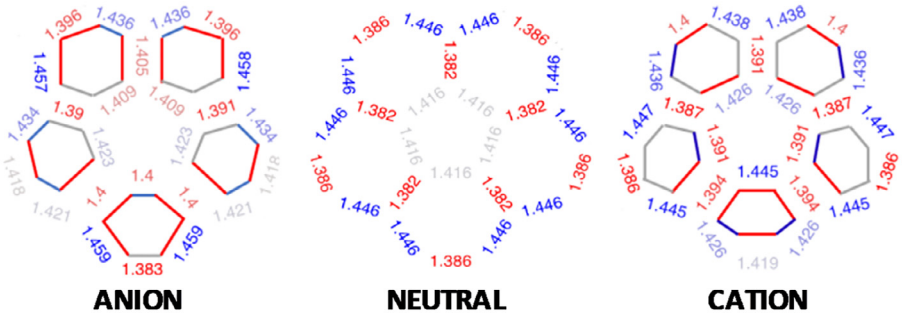

Fig. 3. Bond lengths of JT distorted equilibrium structure (the other four are symmetry-related obtained by C_5 rotations) for corannulene anion (left) and cation (right): The hexagon emphasize the distortion of the rings from the neutral form (blue: shortening, red: lengthening, grey: almost unaffected). The neutral form is shown for reference (centre). (For interpretation of the references to color in this figure legend, the reader is referred to the web version of this article.)

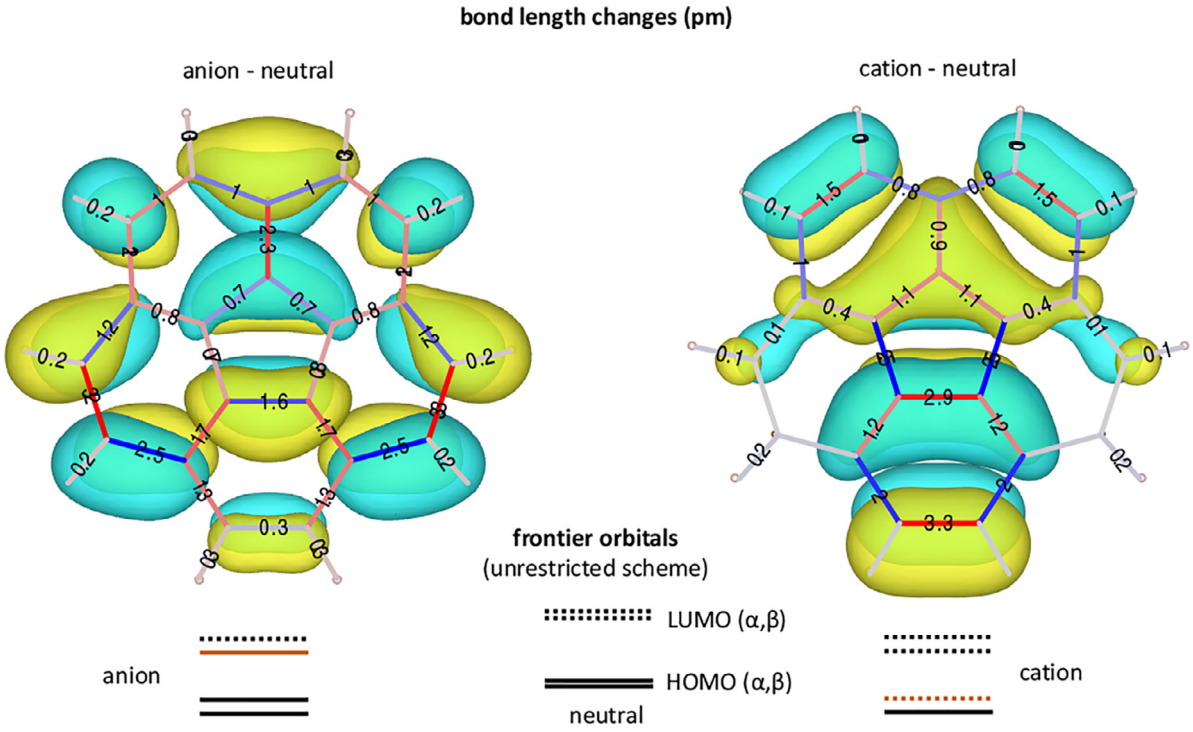

Fig. 4. JT analysis of corannulene anion (left) and cation (right): The variation of the bond length with respect to the neutral form (blue bonds correspond to a shortening, and red bonds to an elongation) is shown. Selected frontier spin-orbitals are shown overlapped with each structure to justify the observed structure relaxation patterns (see text and SI for additional details). The JT distorted structures of the corannulene anion and cation both belongs to the C_s point group symmetry and their electronic wavefunction is 2-A'. (For interpretation of the references to color in this figure legend, the reader is referred to the web version of this article.)

[40]. Our present analysis, based on a Monte Carlo sampling of the PES of the corannulene cation, followed by tight full geometry optimization (see Methods), discards such possibility: no JT distorted stable minimum other than that reported in Fig. 3 was found. Moreover, we carefully checked the JT distorted state identified by the CC bond lengths of the inner pentagon given by 1.384 Å, 1.440 Å, and 1.408 Å (B3LYP/6–311G(d,p) calculation, table II of the paper by Galué et al. [40]). By re-computing Galué structure with tight convergence thresholds, we actually found a first-order saddle point with imaginary frequency of about *i*30 cm^{-1}. This structure is interpreted as the transition state between equivalent JT distorted minima, similar to that found for Cu^{2+} impurities placed in cubic lattices with fluorite structure [51].

It might be convenient to compare the calculated bond lengths of anions with experimental values from the crystals with alkaline counter ions [41] (X-ray diffraction data for the cations of coronene and corannulene could not be found in the literature). We refer the reader to ESI (Tables SI1 and SI2) for further comments.

In IR multiple-photon dissociation (IRMPD) experiments [40] the corannulene cation displays a larger number of IR transitions than the coronene cation, whose position is consistent with DFT calculations (Table 2). Compared with the coronene cation (D_{2h}), the larger number of IR transitions observed in corannulene cation (C_s) is due to the much less symmetric, non-planar structure.

Calculation of EPR parameters

We calculated the *g*-tensors for the optimized geometries of the JT distorted ions, computed at the B3LYP/6–311G(d,p) level which in the previous section was deemed reliable in providing a good description of the vibrational structure of both coronene cation and corannulene cations. Therefore, we kept the same B3LYP functional and considered different basis sets to benchmark the sensitivity (Table 3) with respect to reference experimental EPR data (Table 4). From a quick inspection, it is clear that the 6–311++G(d,p) basis set (including diffuse orbitals),

Table 1
The observed IR transitions of the cation of coronene, compared with present results from DFT calculations. The representation of the normal modes taken from B3LYP/cc-pVTZ results is also provided (this is very close to that of B3LYP/6–311G(d,p) normal modes) (see ESI for the representation of the associated nuclear displacements).

Expt. Matrix [50]	B3LYP/cc-pVTZ (cm^{-1}, km/mol)	B3LYP/6–311G(d,p) (cm^{-1}, km/mol)	irrep	mode description
875	903 (145)	894 (160)	B_{3u}	(a)
1379	1392 (289)	1393 (302)	B_{1u}	(b)
1579	1605 (413)	1605 (426)	B_{1u}	(c)

(a) collective in-phase CH out-of-plane bending.
(b) D-mode displacement of rings (A, B) out-of-phase *vs*. rings (F, G).
(c) G-mode displacement of rings (F, G) out-of-phase *vs*. rings (A, B).

Table 2
The observed IR transitions of the cation of corannulene, compared with present results from DFT calculations (see ESI for the representation of the associated nuclear displacements).

Expt. IRMPD [40]	B3LYP/cc-pVTZ (cm^{-1}, km/mol)	B3LYP/6–311G(d,p) (cm^{-1}, km/mol)	irrep	mode description
835	858 (32)	851 (4)	A”	(a_1)
	860.9 (33)	857.7 (35)	A’	(a_2)
	861.2 (18)	856.3 (50)	A”	(a_3)
	899 (108)	891 (119)	A’	(a_4)
1092	1033 (174)	1031 (175)	A’	(b)
1154	1097 (254)	1096 (227)	A’	(c_1)
	1101 (357)	1101 (365)	A”	(c_2)
	1105 (27)	1101 (63)	A’	(c_3)
1222	1191 (79)	1190 (89)	A’	(d_1)
	1209 (25)	1208 (24)	A’	(d_2)
	1217 (75)	1215 (89)	A”	(d_3)
1332	1292 (118)	1289 (118)	A’	(e_1)
	1303 (178)	1300 (185)	A”	(e_2)
1663	1572 (174)	1571 (174)	A”	(f_1)
	1607 (179)	1606 (180)	A’	(f_2)

(a_1, a_3, a_4) collective CH out-of-plane bending.
(a_2) ring deformation, collective CH out-of-plane bending.
(b) pentagonal ring deformation, CH bending, edge CC stretching.
(c_1, c_2, c_3) collective CC stretching, ring deformation, CH bending.
(d_1, d_2, d_3) collective ring deformation, CH bending.
(e_1, e_2) ring stretching (reminiscent of graphene D mode).
(f_1, f_2) ring stretching (reminiscent of graphene G mode).

Table 3
Calculated energies (*E*), *g*-tensor principal components (in-plane g_1, g_2, and out-of-plane g_Z – with respect to the internal hexagon/pentagon), isotropic value (g_{iso}) and anisotropy parameter (Δg) of the *g*-tensor for the ions of coronene and corannulene.

Ion	Method	*E* (Ha)	g_Z	g_1	g_2	g_{iso}	Δg
coronene (+)	**epr-ii**	−921.15944491	2.0021108	2.0022486	2.0030216	2.0024603	0.0009108
	6–311G(d,p)	−921.26173606	2.0020811	2.0022619	2.0030656	2.0024695	0.0009845
	6–311++G(d,p)	−921.26774108	2.0008139	2.0405486	2.1553143	2.0655589	0.1545004
	cc-pVTZ	−921.35667918	2.0021122	2.0022356	2.0030705	2.0024728	0.0009583
	def2-tzvp	−921.37759747	2.0020988	2.0023057	2.0031360	2.0025135	0.0010372
	def2-tzvpp	−921.38261962	2.0020909	2.0022998	2.0031294	2.0025067	0.0010385
corannulene (+)	**epr-ii**	−767.46893487	2.0022817	2.0022527	2.0027789	2.0024378	0.0005262
	6–311G(d,p)	−767.55746144	2.0022656	2.0022557	2.0028119	2.0024444	0.0005562
	6–311++G(d,p)	−767.56311673	2.0069208	2.0054497	2.0103499	2.0075735	0.0049002
	cc-pVTZ	−767.63612739	2.0022759	2.0022679	2.0028286	2.0024575	0.0005607
	def2-tzvp	−767.65352199	2.0022790	2.0022639	2.0028518	2.0024649	0.0005879
	def2-tzvpp	−767.65763723	2.0022791	2.0022611	2.0028567	2.0024656	0.0005956
coronene (-)	**epr-ii**	−921.42403112	2.0017901	2.0023648	2.0031515	2.0024355	0.0013614
	6–311G(d,p)	−921.52804635	2.0017179	2.0024084	2.0032353	2.0024539	0.0015174
	6–311++G(d,p)	−921.54062213	1.9771523	2.0081684	2.0150916	2.0001374	0.0379393
	cc-pVTZ	−921.62384556	2.0017518	2.0025350	2.0032782	2.0025217	0.0015264
	def2-tzvp	−921.64694093	2.0017270	2.0022032	2.0032696	2.0023999	0.0015426
	def2-tzvpp	−921.65229166	2.0017294	2.0020745	2.0032696	2.0023578	0.0015402
corannulene (-)	**epr-ii**	−767.76064156	2.0013956	2.0024754	2.0029896	2.0022869	0.0015940
	6–311G(d,p)	−767.84982195	2.0011439	2.0025020	2.0030713	2.0022391	0.0019274
	6–311++G(d,p)	−767.86403122	1.9220340	1.9955501	2.0097528	1.9757790	0.0877188
	cc-pVTZ	−767.93034207	2.0011004	2.0025479	2.0031351	2.0022611	0.0020347
	def2-tzvp	−767.95062795	2.0010117	2.0024346	2.0030779	2.0021747	0.0020662
	def2-tzvpp	−767.95505687	2.0010529	2.0024079	2.0030854	2.0021821	0.0020325

Table 4
Experimental *g*-values for the ions of coronene and corannulene.

Ion	Solvent	<g>	Ref.
Coronene (+)	H_2SO_4	2.00256	[52]
	hexafluoroisopropanol/Tl(III) trifluoroacetate	2.00260	[53]
	SbF_5/SO_2ClF/Tl(III) trifluoroacetate	2.00256	[54]
	/	2.0025	[55]
Corannulene (+)	*no experimental data available*		
Coronene (-)	DME/Na	2.003068	[56]
	THF/Na	2.0032	[57]
Corannulene (-)	/	2.0029	[55]
	propylene carbonate	2.0045	[58]
	THF/K, THF/Li	2.0027	[59]
	THF/Li	2.0025	[60]
	THF/Na, THF/K, DME/Alkyl ammonium ions	2.0027	[61]

is totally unsuited, also in anions, where the use of such functions is usually recommended [43]. All other basis sets provide rather similar results, with differences of ±0.0001 for the single principal values of the *g*-components. This accuracy of *g*-values is acceptable, as it is comparable with the accuracy of most EPR measurements. For the sake of completeness, we also checked the *g*-tensor calculations on the JT equilibrium geometries computed with the B3LYP/cc-pVTZ method; the results are reported in ESI (Table SI3) and display very minor differences (of the order of about $\pm 10^{-4}$) with respect to the EPR calculations carried out on B3LYP/6–311G(d,p) equilibrium geometries. The *Z*-direction is taken perpendicular to the π-system in coronene, or perpendicular to the central ring in corannulene. The isotropic values, $g_{iso} = (g_1 + g_2 + g_Z)/3$, are between 2.0024 and 2.0025 for all the ions, but for the corannulene anion we find a slightly smaller value, in the range of 2.0021–2.0023.

Remarkably, the results from 6–311++G(d,p) method are not in line with these values, and well distant from those expected for organic molecules in general, mainly because of an overestimation of the paramagnetic contribution of the spin-orbit term.

We note that the anisotropy, $\Delta g = \max(g_1, g_2, g_Z) - \min(g_1, g_2, g_Z)$, of the cations is smaller than the anisotropy of the anions. Moreover, due to the JT symmetry lowering, in positively and negatively charged ions we obtained tensors with orthorhombic symmetry.

We turn now to the comparison between the theoretical data of Table 3 and the experimental data of Table 4, relative to EPR measurements on fluid solutions. It is convenient to compare first the anions for which the experimental values are available for both coronene and corannulene.

The coronene anion displays a larger g_{iso} value than corannulene, and this experimental trend is reproduced by the calculations. The calculation that deviates the most from the experimental values is that on coronene anion, (0.0007), and the agreement is much better for the corannulene anion. According to the theory by Stone, also extended to degenerate states [37,62], one component (g_Z) is always close to g_e. However, Atkins and Jamieson [63] found that the solution of the Dirac equations bring more terms that justify the deviations from g_e. Indeed, beside the relativistic contribution (−0.00014), along the Z-direction we have both diamagnetic (0.00002–0.00004) and paramagnetic spin-orbit contributions (g_{PSO}) [44].

The calculated terms are reported in the S.I. (Table SI4). In all of the ions, one in-plane component of the g_{PSO} contribution is large and positive. The Z-component is small for the cations (and generally positive), but large and negative for the anions. Therefore, the values in corannulene anion (in the range 2.0010–2.0013) are unexpectedly low. We associate such low values to the presence of the pentagonal ring that induces a curvature to the π-system. For instance, we note that low *g*-components are found in other related carbon structures containing such characteristic moiety, like fullerene-type ions [64]. Finally, we notice that the *g*-value of the coronene cation is reproduced with a remarkable accuracy, while for the anions the relatively small mismatches are likely due to the spin/orbit contributions, which have two relatively large components with opposite sign, a situation that sometimes can induce instability.

The JT distortion of the coronene and corannulene ions has been debated for a long time, and different approaches have been used. Because of the geometry optimization of JT distorted structures discussed above, in our models the JT distortion has been already considered for the interpretation of the EPR measurements. Notably, in a series of papers focused on benzene and coronene anions in solution, the EPR spectra exhibited an unusual line broadening that was attributed to the JT effect [65–67]. However, it was unclear if the broadening was connected to the JT-induced modulation of the hyperfine interactions or to a modulation of the spin/orbit coupling (dynamic JT effect). At that time, the JT distortion was considered in detail for the calculation of the proton hyperfine interactions, but the calculation carried out for the vibronic states showed that a symmetric state is plausible, as the distorted structures are slightly higher in energy, but, apparently, for EPR measurements in solution state, the solvent might play a major role in the stabilization of the JT forms [66].

A different conclusion was obtained by Sato et al. [68] after the analysis of the EPR spectra of the coronene ions that, differently from corannulene, exhibited 13 equally spaced lines down to 203 K that were taken as evidence of no JT distortion associated to the lowering of coronene symmetry. However, in ref. [68] the authors did not carry out a careful linewidth analysis, whereas this kind of analysis was the argument previously assumed in ref. [69] to invoke JT distortion. For corannulene, instead, the same authors concluded that the EPR data show unequivocally that the anion is distorted [69], because at temperatures below 273 K the symmetry of the system is lowered and the EPR spectrum becomes more complex, with a large number of lines due to the presence of inequivalent protons. This was expected in the presence of a dynamic JT effect [70], with a relatively low interconversion barrier between the structures [26]. As a consequence, at high temperature, the fast interconversion between forms averages the hyperfine interactions of all protons, so that they become equivalent [39]. Also, in a previous work by Baumgarten et al. [59], at 200 K the lowering of symmetry was not observed, and consequently the conclusion of the work was that the corannulene anion is highly symmetric.

An issue that is not apparently taken into account in the interpretation of the experimental EPR data is that neutral corannulene is a very flexible aromatic compound capable of performing another conformational change: the bowl-to-bowl inversion, with an estimated energy barrier of 10.2 ± 0.2 kcal/mol (*i.e.*, 3570 ± 70 cm^{-1}) [70]. If the energy barrier is almost the same also for the ions of corannulene, the bowl-to-bowl inversion should also contribute mainly to the relaxation properties of the molecule (spectral linewidth), but it should not affect the molecular magnetic parameters. Unfortunately, the corannulene cation is unstable and it is likely prone to polymerization [61], thus it has not been observed in solution so far.

Different types of calculation have been carried out especially for the anions of corannulene. The JT distortions in the mono anion of corannu-

lene was found to drive a reduction of the symmetry of the radical state from C_{5v} to C_S structures [39,70], in agreement with the results of our work (see Fig. 4). In the work by Sato et al. [70] the energy difference ΔE between the different JT forms and the TS was found to be about 20 cm^{-1}, which also agrees with the value found in [26].

Regarding the calculation of the *g*-tensor, few papers deal with the estimation of this parameter in PAHs, and the first dealing with formally degenerate states was that by Moss and Perry [37], who extended Stone's theory to the case of degenerate states. They considered the case of benzene anion, and coronene as an extension of that case. The calculation was focused on the estimation of its trace, as the available experimental values (see Table 4) were obtained in fluid solution. They recognize the possible splitting of degenerate levels and *g*-factor deviations as due to coupling/combinations of JT inactive vibrations.

Here we claim that several JT distorted structures at the same energy are present, and they are separated by rather low energy barriers, therefore it is likely that these systems are subject to dynamical JT effects.

At the end of this discussion, we point out that other higher order spin–orbit terms for the *g*-tensor could be included in the model, but, so far, these calculations have been limited to small molecules [70].

Conclusions

By DFT calculations we investigated the impact of the Jahn-Teller distortion on the EPR spectroscopy of coronene and corannulene ions. By adopting tight convergence criteria, we have identified robust stable structures (no negative frequencies) of the neutral and JT distorted singly ionized forms of coronene and corannulene, revising and unifying the results available in the literature. A careful Monte-Carlo based optimization of the JT distorted equilibrium structures shows that a manifold of n symmetric replicas of *one single* distorted form is obtained for each ion of the two molecules, with $n = 3$ for coronene and $n = 5$ for corannulene. Based on the analysis of the frontier orbitals we could justify the observed variations of the CC bond lengths while passing from the neutral form to the JT minima. The quite flat energy landscape in the vicinity of the stable minima and the low energy barrier between the JT conformers allows a relatively easy thermally-activated interconversion. *A posteriori*, this supports our choice to run DFT calculations with tight convergence criteria.

The results obtained for the IR transitions of the JT distorted cations of coronene and corannulene satisfactorily reproduce the experimentally available IRMPD data [40]. As for EPR spectroscopy, the calculated *g*-values quantitatively reproduce the experimental values to a satisfactory precision, with the exception of the coronene anion, which displays a too low theoretical value. The computed *g*-tensor of the corannulene anion is of particular interest, since it shows the lowest principal value much smaller than g_e. This result is of particular interest for EPR spectroscopy of graphene-like systems, where low *g*-tensor components have been measured [29].

Finally, the JT distortion and the low activation energy for interconversion between conformers allows to understand the underneath cause of the unusual broadening of the lines of the EPR spectra discussed in the literature as function of temperature (see for instance ref.s [71] and [59]).

The relevant data for the calculations (molecular geometries) are available within the Supporting Information of the manuscript.

Declaration of Competing Interest

There are no conflicts to declare.

Supplementary materials

Supplementary material associated with this article can be found, in the online version, at doi:10.1016/j.chphi.2021.100012.

CRediT authorship contribution statement

Francesco Tampieri: Software, Visualization, Data curtion, Investigation, Writing – review & editing. **Antonio Barbon:** Conceptualization, Supervision, Writing – original draft. **Matteo Tommasini:** Methodology, Software, Conceptualization, Data curtion, Writing – review & editing.

References

[1] E. Clar, The aromatic sextet, in: Mobile Source Emissions Including Policyclic Organic Species, Springer Netherlands, Dordrecht, 1983, pp. 49–58, doi:10.1007/978-94-009-7197-4_4.
[2] G. Trinquier, J.-.P. Malrieu, Predicting the open-shell character of polycyclic hydrocarbons in terms of clar sextets, J. Phys. Chem. A. 122 (2018) 1088–1103, doi:10.1021/acs.jpca.7b11095.
[3] M.A. Dobrowolski, A. Ciesielski, M.K. Cyrański, On the aromatic stabilization of corannulene and coronene, Phys. Chem. Chem. Phys. 13 (2011) 20557, doi:10.1039/c1cp21994d.
[4] Y. Deng, D. Yu, X. Cao, L. Liu, C. Rong, T. Lu, S. Liu, Structure, aromaticity and reactivity of corannulene and its analogues: a conceptual density functional theory and density functional reactivity theory study, Mol. Phys. 116 (2018) 956–968, doi:10.1080/00268976.2017.1403657.
[5] D.M. Hudgins, S.A. Sandford, Infrared spectroscopy of matrix isolated polycyclic aromatic hydrocarbons. 2. PAHs containing five or more rings, J. Phys. Chem. A 102 (1998) 344–352, doi:10.1021/jp983482y.
[6] D.M. Hudgins, S.A. Sandford, Infrared spectroscopy of matrix isolated polycyclic aromatic hydrocarbons. 1. PAHs containing two to four rings, J. Phys. Chem. A 102 (1998) 329–343, doi:10.1021/jp9834816.
[7] D.M. Hudgins, C.W. Bauschlicher, L.J. Allamandola, Closed-shell polycyclic aromatic hydrocarbon cations: a new category of interstellar polycyclic aromatic hydrocarbons, Spectrochim. Acta Part A Mol. Biomol. Spectrosc. 57 (2001) 907–930, doi:10.1016/S1386-1425(00)00453-4.
[8] S.H. Cuylle, L.J. Allamandola, H. Linnartz, Photochemistry of PAHs in cosmic water ice, Astron. Astrophys. 562 (2014) A22, doi:10.1051/0004-6361/201322495.
[9] M. Bahou, Y.-.J. Wu, Y.-.P. Lee, Infrared spectra of protonated coronene and its neutral counterpart in solid parahydrogen: implications for unidentified interstellar infrared emission bands, Angew. Chem. Int. Ed. 53 (2014) 1021–1024, doi:10.1002/anie.201308971.
[10] G. Rouillé, C. Jäger, M. Steglich, F. Huisken, T. Henning, G. Theumer, I. Bauer, H.-.J. Knölker, IR, Raman, and UV/Vis spectra of corannulene for use in possible interstellar identification, ChemPhysChem 9 (2008) 2085–2091, doi:10.1002/cphc.200800387.
[11] A.K. Haritash, C.P. Kaushik, Biodegradation aspects of polycyclic aromatic hydrocarbons (PAHs): a review, J. Hazard. Mater. 169 (2009) 1–15, doi:10.1016/j.jhazmat.2009.03.137.
[12] C.D. Schmidt, N. Lang, N. Jux, A. Hirsch, A facile route to water-soluble coronenes and benzo[ghi]perylenes, Chem. A Eur. J. 17 (2011) 5289–5299, doi:10.1002/chem.201003232.
[13] T. Bauert, L. Zoppi, G. Koller, J.S. Siegel, K.K. Baldridge, K.-.H. Ernst, Quadruple anionic buckybowls by solid-state chemistry of corannulene and cesium, J. Am. Chem. Soc. 135 (2013) 12857–12860, doi:10.1021/ja4063103.
[14] M. Yamada, S. Tashiro, R. Miyake, M. Shionoya, A cyclopalladated complex of corannulene with a pyridine pendant and its columnar self-assembly, Dalt. Trans. 42 (2013) 3300, doi:10.1039/c2dt32883f.
[15] J.-.L. Brédas, D. Beljonne, V. Coropceanu, J. Cornil, Charge-transfer and energy-transfer processes in π-conjugated oligomers and polymers: a molecular picture, Chem. Rev. 104 (2004) 4971–5004, doi:10.1021/cr040084k.
[16] X. Feng, W. Pisula, K. Müllen, Large polycyclic aromatic hydrocarbons: synthesis and discotic organization, Pure Appl. Chem. 81 (2009) 2203–2224, doi:10.1351/PAC–CON-09-07-07.
[17] K. Müllen, Evolution of graphene molecules: structural and functional complexity as driving forces behind nanoscience, ACS Nano 8 (2014) 6531–6541, doi:10.1021/nn503283d.
[18] Y. Yamamoto, T. Fukushima, Y. Suna, N. Ishii, A. Saeki, S. Seki, S. Tagawa, M. Taniguchi, T. Kawai, T. Aida, Photoconductive coaxial nanotubes of molecularly connected electron donor and acceptor layers, Science 80- (314) (2006) 1761–1764, doi:10.1126/science.1134441.
[19] A.K. Geim, Random walk to graphene (nobel lecture), Angew. Chem. Int. Ed. 50 (2011) 6966–6985, doi:10.1002/anie.201101174.
[20] A. Barbon, EPR spectroscopy in the study of 2D graphene-based nanomaterials and nanographites, in: V. Chechik, D.M. Murphy (Eds.), Specialist Periodical Reports Electron Paramagnetic Resonance, Royal Society of Chemistry, 2018, pp. 38–65, doi:10.1039/9781788013888-00038.
[21] A. Narita, X.-.Y. Wang, X. Feng, K. Müllen, New advances in nanographene chemistry, Chem. Soc. Rev. 44 (2015) 6616–6643, doi:10.1039/C5CS00183H.
[22] W. Yang, G. Longhi, S. Abbate, A. Lucotti, M. Tommasini, C. Villani, V.J. Catalano, A.O. Lykhin, S.A. Varganov, W.A. Chalifoux, Chiral peropyrene: synthesis, structure, and properties, J. Am. Chem. Soc. 139 (2017) 13102–13109, doi:10.1021/jacs.7b06848.
[23] N. Kheirabadi, A. Shafiekhani, The ground state of graphene and graphene disordered by vacancies, Phys. E Low Dimens. Syst. Nanostruct. 47 (2013) 309–315, doi:10.1016/j.physe.2012.09.022.

[24] V. Tozzini, V. Pellegrini, Electronic structure and Peierls instability in graphene nanoribbons sculpted in graphane, Phys. Rev. B 81 (2010) 113404, doi:10.1103/PhysRevB.81.113404.
[25] A. Santana, A.M. Popov, E. Bichoutskaia, Stability and dynamics of vacancy in graphene flakes: edge effects, Chem. Phys. Lett. 557 (2013) 80–87, doi:10.1016/j.cplett.2012.11.077.
[26] L. Andjelković, M. Gruden-Pavlović, M. Zlatar, Density functional theory study of the multimode Jahn–Teller problem in the open-shell corannulenes and coronenes, Chem. Phys. 460 (2015) 64–74, doi:10.1016/j.chemphys.2015.05.007.
[27] M. Tommasini, C. Castiglioni, G. Zerbi, Raman scattering of molecular graphenes, Phys. Chem. Chem. Phys. 11 (2009) 10185, doi:10.1039/b913660f.
[28] F. Tampieri, A. Barbon, Resolution of EPR signals in graphene-based materials from few layers to nanographites, in: D. Savchenko, A.H. Kassiba (Eds.), Frontiers in Magnetic Resonance Electron Paramagnetic Resonance in Modern Carbon-Based Nanomaterials, Bentham Science, 2018, pp. 36–66, doi:10.2174/9781681086934118010005.
[29] F. Tampieri, S. Silvestrini, R. Riccò, M. Maggini, A. Barbon, A comparative electron paramagnetic resonance study of expanded graphites and graphene, J. Mater. Chem. C 2 (2014) 8105–8112, doi:10.1039/C4TC01383B.
[30] A. Barbon, F. Tampieri, Identification of slow relaxing spin components by pulse EPR techniques in graphene-related materials, AIMS Mater. Sci. 4 (2017) 147–157, doi:10.3934/matersci.2017.1.147.
[31] C.N.R. Rao, A.K. Sood (Eds.), Graphene: Synthesis, Properties, and Phenomena, Wiley-VCH Verlag GmbH & Co. KGaA, Weinheim, Germany, 2013, doi:10.1002/9783527651122.
[32] M. Tommasini, C. Castiglioni, G. Zerbi, A. Barbon, M. Brustolon, A joint Raman and EPR spectroscopic study on ball-milled nanographites, Chem. Phys. Lett. 516 (2011) 220–224, doi:10.1016/j.cplett.2011.09.094.
[33] A. Barbon, M. Brustolon, An EPR study on nanographites, Appl. Magn. Reson. 42 (2012) 197–210, doi:10.1007/s00723-011-0285-6.
[34] V.L.J. Joly, K. Takahara, K. Takai, K. Sugihara, T. Enoki, M. Koshino, H. Tanaka, Effect of electron localization on the edge-state spins in a disordered network of nanographene sheets, Phys. Rev. B 81 (2010) 115408, doi:10.1103/PhysRevB.81.115408.
[35] Ł. Majchrzycki, M.A. Augustyniak-Jabłokow, R. Strzelczyk, M. Maćkowiak, Magnetic centres in functionalized graphene, Acta Phys. Pol. A 127 (2015) 540–542, doi:10.12693/APhysPolA.127.540.
[36] T.L. Makarova, A.L. Shelankov, A.I. Shames, A.A. Zyrianova, A.A. Komlev, G.N. Chekhova, D.V. Pinakov, L.G. Bulusheva, A.V. Okotrub, E. Lähderanta, Tabby graphene: dimensional magnetic crossover in fluorinated graphite, Sci. Rep. 7 (2017) 16544, doi:10.1038/s41598-017-16321-5.
[37] R.E. Moss, A.J. Perry, g -factor deviations in degenerate aromatic hydrocarbon radicals: the benzene anion, Mol. Phys. 22 (1971) 789–798, doi:10.1080/00268977100103111.
[38] T. Kato, K. Yoshizawa, T. Yamabe, Jahn–Teller effects in the coronene anions and cations, J. Chem. Phys. 110 (1999) 249–255, doi:10.1063/1.478100.
[39] T. Yamabe, K. Yahara, T. Kato, K. Yoshizawa, Vibronic coupling and Jahn–Teller effects in negatively charged corannulene, J. Phys. Chem. A 104 (2000) 589–595, doi:10.1021/jp992496g.
[40] H.A. Galué, C.A. Rice, J.D. Steill, J. Oomens, Infrared spectroscopy of ionized corannulene in the gas phase, J. Chem. Phys. 134 (2011) 054310, doi:10.1063/1.3540661.
[41] A.S. Filatov, N.J. Sumner, S.N. Spisak, A.V. Zabula, A.Y. Rogachev, M.A. Petrukhina, Jahn-Teller effect in circulenes: x-ray diffraction study of coronene and corannulene radical anions, Chem. A Eur. J. 18 (2012) 15753–15760, doi:10.1002/chem.201202026.
[42] G. Marsaglia, Choosing a point from the surface of a sphere, Ann. Math. Stat. 43 (1972) 645–646, doi:10.1214/aoms/1177692644.
[43] F. Jensen, Introduction to Computational Chemistry, 3rd ed., John Wiley & Sons, 2016.
[44] F. Neese, The ORCA program system, WIREs Comput. Mol. Sci. 2 (2012) 73–78, doi:10.1002/wcms.81.
[45] G.L. Stoychev, A.A. Auer, R. Izsák, F. Neese, Self-consistent field calculation of nuclear magnetic resonance chemical shielding constants using gauge-including atomic orbitals and approximate two-electron integrals, J. Chem. Theory Comput. 14 (2018) 619–637, doi:10.1021/acs.jctc.7b01006.
[46] E. Fawcett, J. Trotter, The crystal and molecular structure of coronene, Proc. R. Soc. Lond. Ser. A Math. Phys. Sci. 289 (1966) 366–376, doi:10.1098/rspa.1966.0017.
[47] S.R. Langhoff, Theoretical infrared spectra for polycyclic aromatic hydrocarbon neutrals, cations, and anions, J. Phys. Chem. 100 (1996) 2819–2841, doi:10.1021/jp952074g.
[48] J. Oomens, B.G. Sartakov, A.G.G.M. Tielens, G. Meijer, G. von Helden, Gas-phase infrared spectrum of the coronene cation, Astrophys. J. 560 (2001) L99–L103, doi:10.1086/324170.
[49] L.J. Allamandola, G.G.M. Tielens, J.R. Barker, Interstellar polycyclic aromatic hydrocarbons - The infrared emission bands, the excitation/emission mechanism, and the astrophysical implications, Astrophys. J. Suppl. Ser. 71 (1989) 733, doi:10.1086/191396.
[50] D.M. Hudgins, L.J. Allamandola, Infrared spectroscopy of matrix-isolated polycyclic aromatic hydrocarbon cations. 2. The members of the thermodynamically most favorable series through coronene, J. Phys. Chem. 99 (1995) 3033–3046, doi:10.1021/j100010a011.
[51] M. Moreno, M.T. Barriuso, J.A. Aramburu, P. García-Fernández, J.M. García-Lastra, Microscopic insight into properties and electronic instabilities of impurities in cubic and lower symmetry insulators: the influence of pressure, J. Phys. Condens. Matter. 18 (2006) R315–R360, doi:10.1088/0953-8984/18/17/R01.
[52] H. van Willigen, E. de Boer, J.T. Cooper, W.F. Forbes, ESR study of the dimer cation of coronene, J. Chem. Phys. 49 (1968) 1190–1192, doi:10.1063/1.1670208.
[53] K. Komaguchi, K. Nomura, M. Shiotani, A. Lund, M. Jansson, S. Lunell, ESR and theoretical studies of trimer radical cations of coronene, Spectrochim. Acta Part A Mol. Biomol. Spectrosc. 63 (2006) 76–84, doi:10.1016/j.saa.2005.04.039.
[54] P.J. Krusic, E. Wasserman, Coronene dication: a thermally accessible triplet, J. Am. Chem. Soc. 113 (1991) 2322–2323, doi:10.1021/ja00006a072.
[55] Blois M.S., Brown H.W., Maling J.E., Free Radicals in Biological Systems, Academic Press, New York, 1961, p. 117.
[56] B.G. Segal, M. Kaplan, G.K. Fraenkel, Measurement of g values in the electron spin resonance spectra of free radicals, J. Chem. Phys. 43 (1965) 4191–4200, doi:10.1063/1.1696676.
[57] M. Sato, K. Yamamoto, H. Sonobe, K. Yano, H. Matsubara, H. Fujita, T. Sugimoto, K. Yamamoto, Convenient synthesis and reduction properties of [7]circulene, J. Chem. Soc. Perkin Trans. 2 (1998) 1909–1914, doi:10.1039/a803306d.
[58] R.J. Angelici, B. Zhu, S. Fedi, F. Laschi, P. Zanello, Electrochemical and EPR studies of the corannulene ruthenium(II) sandwich complex $[(\eta^6\text{-}C_6Me_6)Ru(\eta^6\text{-}C_{20}H_{10})](SbF_6)_2$, Inorg. Chem. 46 (2007) 10901–10906, doi:10.1021/ic7015512.
[59] M. Baumgarten, L. Gherghel, M. Wagner, A. Weitz, M. Rabinovitz, P.-.C. Cheng, L.T. Scott, Corannulene reduction: spectroscopic detection of all anionic oxidation states, J. Am. Chem. Soc. 117 (1995) 6254–6257, doi:10.1021/ja00128a012.
[60] G. Zilber, V. Rozenshtein, P.-.C. Cheng, L.T. Scott, M. Rabinovitz, H. Levanon, Electron spin dynamics of photoexcited corannulene-lithium complexes in tetrahydrofuran. Fourier transform electron paramagnetic resonance, J. Am. Chem. Soc. 117 (1995) 10720–10725, doi:10.1021/ja00148a014.
[61] J. Janata, J. Gendell, C.-.Y. Ling, W.E. Barth, L. Backes, H.B. Mark, R.G. Lawton, Concerning the anion and cation radicals of corannulene, J. Am. Chem. Soc. 89 (1967) 3056–3058, doi:10.1021/ja00988a050.
[62] A.J. Stone, g tensors of aromatic hydrocarbons, Mol. Phys. 7 (1964) 311–316, doi:10.1080/00268976300101081.
[63] P.W. Atkins, A.M. Jamieson, Perturbation corrections to the g tensor, Mol. Phys. 14 (1968) 425–431, doi:10.1080/00268976800100531.
[64] A. Zoleo, A.L. Maniero, M. Bellinazzi, M. Prato, T. Da Ros, L.C. Brunel, M. Brustolon, Radical anions of fullerene bisadducts: a multifrequency CW-EPR study, J. Magn. Reson. 159 (2002) 226–236, doi:10.1016/S1090-7807(02)00032-0.
[65] M.G. Townsend, S.I. Weissman, Possible symptom of the Jahn-Teller effect in the negative ions of coronene and triphenylene, J. Chem. Phys. 32 (1960) 309–310, doi:10.1063/1.1700934.
[66] H.M. McConnell, A.D. McLachlan, Nuclear hyperfine interactions in orbitally degenerate states of aromatic ions, J. Chem. Phys. 34 (1961) 1–12, doi:10.1063/1.1731545.
[67] I.C. Lewis, L.S. Singer, Electron spin resonance of radical cations produced by the oxidation of aromatic hydrocarbons with $SbCl_5$, J. Chem. Phys. 43 (1965) 2712–2727, doi:10.1063/1.1697200.
[68] T. Sato, H. Tanaka, A. Yamamoto, Y. Kuzumoto, K. Tokunaga, Jahn–Teller effect in coronene monoanion: a comparative study with corannulene monoanion, Chem. Phys. 287 (2003) 91–102, doi:10.1016/S0301-0104(02)00981-3.
[69] T. Sato, A. Yamamoto, H. Tanaka, An ESR study on Jahn–Teller effect in corannulene monoanion, Chem. Phys. Lett. 326 (2000) 573–579, doi:10.1016/S0009-2614(00)00759-4.
[70] T. Sato, A. Yamamoto, T. Yamabe, Electronic and vibrational structures of corannulene anions, J. Phys. Chem. A 104 (2000) 130–137, doi:10.1021/jp992912x.
[71] J.R. Bolton, A. Carrington, The effects of orbital degeneracy in the E.S.R. spectrum of the coronene positive ion, Mol. Phys. 4 (1961) 271–272, doi:10.1080/00268976100100401.